Analysis of the Muon/Electron Ratio in EAS

J.H.Weber[1*], T. Antoni[2], W.D. Apel[2], F. Badea[3], K. Bekk[2], K. Bernlöhr[2], E. Bollmann[2], H. Bozdog[3], I.M. Brancus[3], A. Chilingarian[4], K. Daumiller[1], P. Doll[2], J. Engler[2], F. Feßler[2], H.J. Gils[2], R. Glasstetter[1], R. Haeusler[2], W. Hafemann[2], A. Haungs[2], D. Heck[2], J.R. Hörandel[1‡], T. Holst[2], K.-H. Kampert[1,2] J. Kempa[5], H.O. Klages[2], J. Knapp[1§], H.J. Mathes[2], H.J. Mayer[2], J. Milke[2], D. Mühlenberg[2], J. Oehlschläger[2], M. Petcu[3], H. Rebel[2], M. Risse[2], M. Roth[2], G. Schatz[2], H. Schieler[2], F.K. Schmidt[1], T. Thouw[2], H. Ulrich[2], A. Vardanyan[4], B. Vulpescu[3], J. Wentz[2], T. Wibig[5], T. Wiegert[2], D. Wochele[2], J. Wochele[2], J. Zabierowski[6]

[1] *Institut für Experimentelle Kernphysik, University of Karlsruhe, D-76021 Karlsruhe, Germany*

[2] *Institut für Kernphysik, Forschungszentrum Karlsruhe, D-76021 Karlsruhe, Germany*

[3] *National Institute of Physics and Nuclear Engineering, RO-7690 Bucharest, Romania*

[4] *Cosmic Ray Division, Yerevan Physics Institute, Yerevan 36, Armenia*

[5] *Department of Experimental Physics, University of Lodz, PL-90950 Lodz, Poland*

[6] *Soltan Institute for Nuclear Studies, PL-90950 Lodz, Poland*

Abstract

The detector array of the KASCADE experiment measures the electromagnetic and muonic component of extended air showers. More than 100 million air showers have been analysed in narrow zenith angle bins. The muon number in extended air showers enables a good estimation of the energy of the primary particles, while the number of electrons in the shower depends strongly on the mass of the primary particle as well as on the primary energy and the zenith angle of the event. The reconstructed muon and electron numbers for each event are converted into primary energy using the results of MC-simulations (CORSIKA). The distributions of the muon/electron ratio within small energy bins are compared with the predictions for primary particles of different masses. An energy dependant mass composition was obtained favouring a decrease of light elements above the knee.

1 Experimental Setup and Observables

For the measurement of lateral electron and muon distributions the detector array of the KASCADE experiment comprises about 500 m^2 electron and 620 m^2 muon detectors which are distributed over 252 detector stations (Klages, 1997). The stations house electron detectors and muon detectors that are shielded by slabs of lead and iron. The measured energy deposits in both detector types are corrected to the mutual deposits of all other particles in an extensive air shower to obtain correct electron and muon numbers. This correction is done with lateral correction functions, that mainly depend on primary energy and zenith angle. These functions are based on simulations with the CORSIKA event generator (Heck,1998) followed by a tracking to the KASCADE experiment at observation level. This allows to convert energy deposits into particle numbers using an iterative method.

2 Determination of Electron and Muon Numbers

The data evaluation is performed in 3 levels. In a first level shower core, zenith angle, electron and muon sizes are estimated using short algorithms. The obtained parameters are used to apply the correction functions in a first way and to give start parameters for fits in the following level. A conus fit to the arrival times of the electrons gives the zenith angle. The lateral electron distributions are fitted with a NKG function using a Moliere radius of 89 m that describes the data best. This fit gives the core position and the form parameter (age) of the distribution, too. The lateral muon distribution is fitted with a NKG function as well, using a

[*] corresponding author; e-mail: weber@ik1.fzk.de

[‡] present address: University of Chicago, Enrico Fermi Institute, Chicago, IL 60637

[§] now at: University of Leeds, Leeds LS2 9JT, U.K.

Moliere radius of 420 m in a fit range of 40 m - 200 m. The lower cut is due to uncorrectable punch through from hadrons and photons in the muon detectors near the shower core. This fit uses the shower core obtained by the previous fit and a parametrization of the muon form parameter (age$_\mu$) as a function of the electron size. This parametrization is obtained from simulations. In a third level a combined fit to the lateral electron distribution is performed using the fit result of the lateral muon distribution as a background function. With the knowledge of the lateral electron distribution the deposit in the muon detectors is corrected again and the resulting lateral distribution is fitted again. The muon distribution is integrated within the fit range of 40 m - 200 m resulting in the truncated muon number N_μ^{tr}. This parameter has the advantage to be free of systematical errors caused by extrapolations outside the experimentel acceptance and is in addition a good estimator of the primary energy irrespective of the primary mass. The electron size and the truncated muon size can be obtained with a systematic error less then $\sim 8\%$.

3 Determination of the Mass Composition with the Muon/Electron Ratio

The data presented here were taken out of $\sim$ 140 million reconstructed events. Several cuts were applied to the reconstructed events in order to ensure reliable results. An energy threshold of $\sim 10^{15}$ eV guarantees 100% trigger and reconstruction effciency. Due to the influence of the atmospherical depth on the shower parameters the data were subdivided into narrow zenith angle bins. To be comparable with simulations the zenith angle of the data shown in all following figures was restricted to $18^o < \theta < 25^o$. The resulting sample consists of 380.000 measured events after all cuts. As simulations with the hadronic interaction model QGSJET turned out to show the best agreement with the data analysis using this model only will be presented. All simulated showers have been tracked through the experiment und reconstructed like the measured data, so systematic errors due to the reconstruction methods can be neglected. The simulated showers have been given a weigth in energy corresponding to the mesured energy flux. In a first step the data were divided into 12 energy intervals in a range from $5.9 \leq \log(E_o/\mathrm{GeV}) \leq 7.1$. The energy binning is performed according to a function of the muon size N_μ^{tr} and the electron size N_e as obtained from simulations. The muon size is the dominant energy estimator while the electron size is used as a small correction to reduce the slight mass dependance of N_μ^{tr}. Figure 1 shows the quality of the energy reconstruction. The line indicates a perfect reconstruction accuracy. Systematic errors in the energy determination between proton and iron induced showers are not larger then the energy intervals. The error bars represent the spread of the reconstructed energy that mainly results from the spread in muon and electron sizes themselves. The good reconstruction accuracy implements the possibilty to divide the data in nearly mass-independant energy intervalls without prior knowledge of the mass composition.

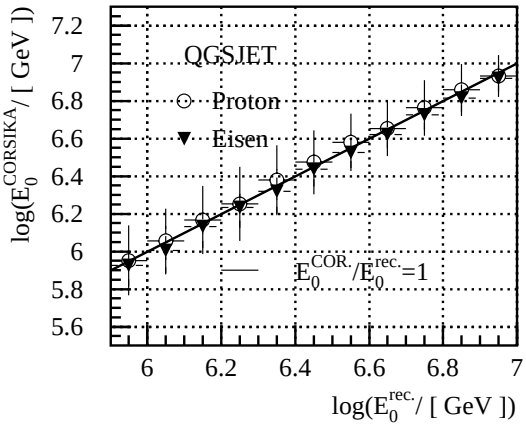

Figure 1: The primary energy from simulations as function of the reconstructed energy for proton and iron induced showers.

The ratio $\log(N_\mu^{tr})/\log(N_e)$ has been found to be the most sensitive mass parameter. The distributions of

this parameter can be described in good approximation with a Gaussian function. The mean values and spread of the distributions of four mass groups (proton, helium, oxygen, and iron) were parametrized as functions of the reconstruced energy. The sum of these four functions was fitted for each energy bin to the data distribution giving directly the fractions of the 4 mass groups as the fit result. Figure 2 shows two examples of such a fit for energy bin (a) $6.2 < \log(E_0/\mathrm{GeV}) < 6.3$ and (b) $6.7 < \log(E_0/\mathrm{GeV}) < 6.8$ on a logarithmic scale. The points represent the data, the black line represents the fit and the lines from light to dark grey show the simulated distributions of the mass groups (from proton to iron) normalized to the fit result. The figure reveals a very good agreement between the fit and the measured data. No shift of the simulations to one side of the data distribution or an error in the total integral can be found. The relative fractions of the four mass groups for all energy bins are shown in Figure 3 a).

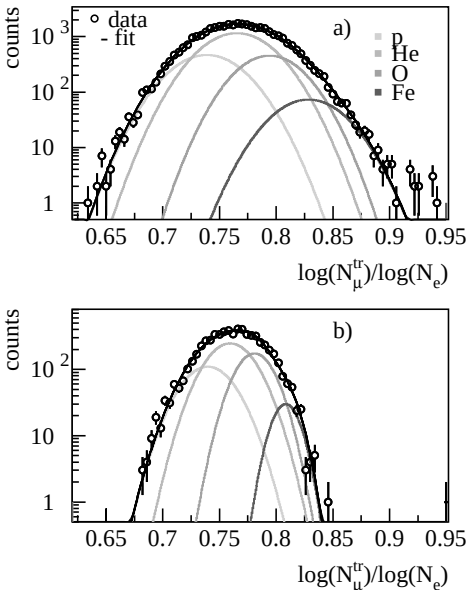

Figure 2: The muon/electron ratio for two different energy bins

4 The Mass Composition

The light grey area indicates the fraction of proton induced showers. The colours darken with increasing mass up to iron induced showers. There is little change in the composition which is clearly light mass dominated up to an energy at 6.5-6.6 $\log(E_0/\mathrm{GeV})$ After that energy which corresponds to the knee position of the all-particle spectrum the composition shows a decrease of light elements with increasing energy. In order to compare our result with other experiments we calculated a mass parameter λ that is defined as $\lambda = \sum_{i=p,He,O,Fe}^{i} ln(A_i) \cdot P_i$ with P_i being the relative fraction of mass group i. The mass parameter is about 1.4 ± 0.3 below the knee and increases to 2.1 ± 0.3 at 10^{16} eV as shown in Figure 3 b). The shaded area represents the systematical uncertainties that result from the Gaussian parametrization of the simulated distributions. Due to the (relative to measured data) small statistics of the simulated showers the widths of the distributions shown in Figure 2 are not very accurately known, resulting in a systematical dependency of the resulting mass parameter. The statistical error of the data can be neglected.

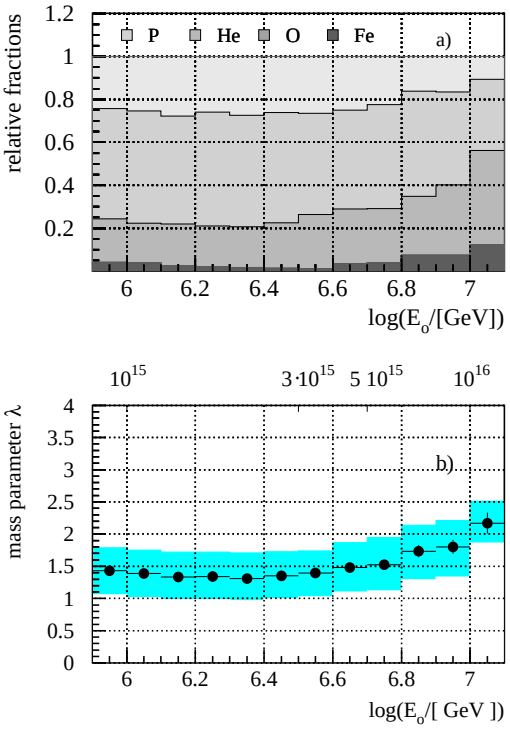

Figure 3: The mass composition (a) and the mass parameter λ (b) as function of the energy

For the following analysis of the primary all-particle flux the data were divided into a light mass group (protons and helium) and a heavy mass group (oxygen and iron). The spectrum was obtained straight forward by using the counts in the energy bins. Small changes of the energy axis due to the steep slope of the energy spectrum have been taken into account. This differential spectrum was weighted once with the percentage of the light mass group and once with that of the heavy mass group. The result is shown in Figure 4. The overall spectrum is plotted in the same figure. It shows clearly a knee position at 6.5-6.6 in $\log(E_0/\mathrm{GeV})$ (corresponding to 3.2-4 $\cdot 10^{15}$ eV) as one would expect from Figure 3 and 4.

The light and heavy mass groups have comparable slopes up to the knee region, but beyond this energy the light mass group shows a significant increase in the slope, while the slope of the heavy mass group remains nearly unchanged. The knee position and the slopes before and after the knee have been fitted using a function described in (Glasstetter,1998). This leads to following results: The knee position is found at 3.7 PeV. The index before the knee is about 2.65 and 2.93 after the knee. The systematic errors we estimate to approximately 13%. The knee position of the light mass group is at a comparable region while the heavy mass group shows no significant knee. The index of the light mass group changes from 2.67 to 3.31, the index of the heavy mass group stays constant at 2.51 The large errors are due to the systematical uncertainties, illustrated in Figure 4 by the shaded area.

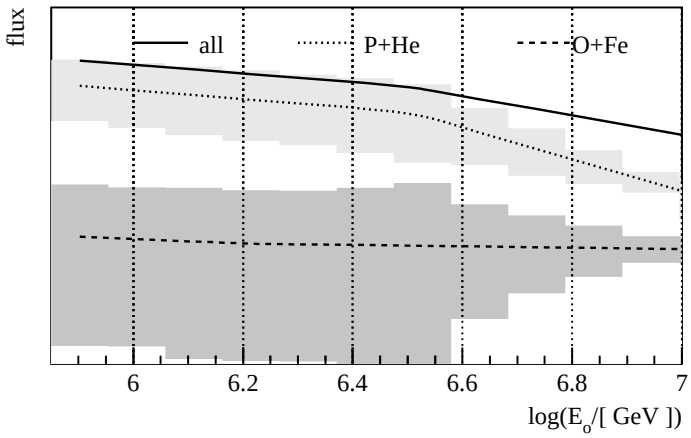

Figure 4: The flux (arbitrary units) for light and heavy masses as function of the energy. The ordinate is multiplied by a factor of $E_0^{2.5}$ to illustrate the shape of the spectrum.

5 Conclusions and Outlook

The spectrum parameter obtained with the hadronic interaction model QGSJET compare well with world data (Watson, 1997). The results of the analysis are in good agreement with acceleration/propagation models where spectra features are functions of the rigidity (Wiebel-Sooth, 1998).

In comparision to direct measurements at lower energies the mass composition obtained appears somewhat biased towards the light mass group. The ratio of the logarithmic sizes is a very sensitive parameter. Though the simulations give a well defined mean of this parameter a shift of the mean by only 2 % (that means $\sim 15\%$ less electrons or $\sim 15\%$ more muons) can change the value of the mass parameter λ from 1.4 to a value of 1.8 at 1 PeV which one would extrapolate from direct measurements. Due to the iterative corrections of the lateral electron distributions with the extrapolated lateral distributions of the muons, that are only defined in a region of 40 m - 200 m, the parametrization of the muon form parameter age$_\mu$ as a function of the electron size (see section 2) becomes a crucial point. Though the simulated parametrization fits the data reasonably within the fit region, a fit to the mean measured lateral distributions, that are collected as a function of the truncated muon size, gives a slightly different age$_\mu$. In a further analysis the parametrization of the muon age will be obtained from the data and not from simulations. First studies with low statistic show a an increase of the ratio of $\sim 1\%$. A careful study of this effect continues.

References

Heck, D. et al., 1998, FZKA 6019 Forschungszentrum Karsruhe (1998)

Glasstetter, R. et al., Proc. 25th ICRC (Durban 1997), 157

Klages, H.O. et al., Nucl. Phys. B (Proc Suppl.) 52b (1997) 922

Watson, A.A., Proc. 25th ICRC (Durban 1997) 8, 257

Wiebel-Sooth, B. et al, A & A, 330 (1998) 389-398